JOURNAL OF MATERIALS SCIENCE 24 (1989) 1077–1088

A tensorial representation of the dissolution slowness: Application to etched singly rotated quartz plates

C. R. TELLIER, J. L. VATERKOWSKI
Laboratoire de Chronométrie, Electronique et Piézoélectricité, Ecole Nationale Supérieure de Mécanique et des Microtechniques, Route de Gray, La Bouloie, 25030 Besancon Cedex, France

A tensorial method is used to determine the equation of the representative surface of the dissolution slowness vector from a vectorial analysis of the dissolution which in three dimensions is described in terms of an orientation dependent dissolution slowness vector. Calculations are derived for the trigonal class 32 and applied to singly rotated quartz crystals for which coefficients are evaluated up to the 16th order. The polar diagram of the dissolution slowness is presented for orientations, θ, in the range $[-60°, 60°]$. A numerical simulation of the dissolution based on the vectorial analysis is used to undertake a systematic comparison of the shape of the theoretical dissolution profiles with the experimental Z' traces of differently oriented singly rotated quartz plates. For BT-cut plates an excellent agreement is found between theoretical and experimental results. For the AT-cut plates with $\theta < 29°$ the agreement is not so good. However, since these AT plates are cut in various quartz crystals the deviation may be attributed to dispersion in the measurement of the etch rate. Thus combining the vectorial analysis of the dissolution with a tensorial representation of the slowness surface provides a useful method for accurately determining the shape of the dissolution profiles of quartz crystals.

1. Introduction

In the past few years chemical etching [1–7] has been studied as an alternative procedure to prepare high-frequency quartz resonators. As compared with the mechanical lapping process which creates a damaged surface layer [1, 8, 9] chemical etching has the advantage of preventing misorientation of the surface of quartz crystals.

However, some previous studies [10–17] on singly and doubly rotated quartz plates immersed in a concentrated $NH_4F \cdot HF$ solution provided evidence for a rapid variation in etch rate and in the shape of dissolution figures with orientation. Moreover, Tellier *et al.* [18] showed that the initial surface damage has no influence on the final texture of deeply etched quartz plates which is determined primarily by the crystal orientation and by the degree of perfection of the bulk structure. These observations have encouraged these authors [19, 20] to develop a numerical simulation of the dissolution derived from the kinematic model [21–23] originally given by Lighthill and Whitman [22]. This bi-dimensional model has been confirmed by experimental results [19, 20] on the topography of the dissolution profiles of singly rotated quartz plates.

Hence, recently [24] a vectorial analysis of the dissolution problem was proposed and the result is that to determine the trajectory of a moving surface profile element we need to know the polar diagram of a vector which characterizes the dissolution, namely the slowness dissolution vector, $\boldsymbol{L}$. Now one may expect to predict the shape of the dissolution profiles of differently oriented quartz plates from the experimental polar diagram of $\boldsymbol{L}$. Consequently the present work continues along this specific line and presents a tensorial method for obtaining the mathematical equation concerning this polar diagram. The mathematical method is reported and a systematic comparison of the theoretical predictions of the simulation with the experimental changes of Z' surface profiles of singly rotated quartz plates on orientation is undertaken.

2. Theoretical

2.1. The dynamical model of the dissolution

In this section we are concerned with a brief presentation of the relevant results of a vectorial analysis of the dissolution which has been described elsewhere [24]. In the first step the main features of the mathematical model are directly derived from the kinematic wave theory previously explored by Lighthill [22] and later by Frank [23]. These features can be characterized as follows. Let a rotated crystal plate of given orientation be the reference surface which lies parallel to the x_2x_3 plane and consider the cross section of a crystal surface presented in Fig. 1. The surface profile is supposed to be composed of a succession of linear profile elements, $\Delta r(\alpha)$, α is the angle from the

0022–2461/89 $03.00 + .12

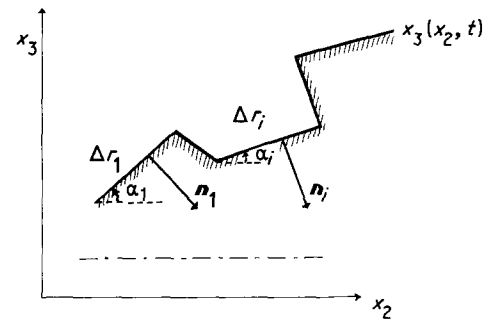

Figure 1 Representation of the surface profile. (–·–·– denotes reference).

reference surface. During the chemical attack a surface profile element of slope $p = (\partial x_3/\partial x_2)_t$ moves within the bulk crystal with a velocity v_3 normal to the reference surface given by

$$v_3 = \left(\frac{\partial x_3}{\partial t}\right)_{x_2} \tag{1}$$

If we express the moving surface profile $x_3(x_2, t)$ as a function of two independent variables the coordinate x_2 and the etching time t we get

$$\mathrm{d}x_3 = p\,\mathrm{d}x_2 + v_3\,\mathrm{d}t \tag{2}$$

Further by using the continuity equation [22, 24] we can show, *under the assumption that the velocity v_3 depends only on the local slope p* i.e. on the local orientation α of the surface profile, that a surface profile element of given slope p propagates into the bulk along a linear trajectory called a characteristic. We can construct the characteristic trajectory of a profile element taking into account the following features

(1) The slope of the characteristic is given by

$$\frac{\mathrm{d}x_3}{\mathrm{d}x_2} = p - \frac{v_3}{(\partial v_3/\partial p)} \tag{3}$$

(2) The position x_2 of the profile element of slope p satisfies the relation

$$\frac{\mathrm{d}x_2}{\mathrm{d}t} = -\frac{\partial v_3}{\partial p} \tag{4}$$

Thus after an etching time $\mathrm{d}t$ the initial element located at M (Fig. 2) has progressed into the bulk crystal in such a way it is now located at M′ where MM′ represents a vector, denoted for convenience by the propagation vector $\boldsymbol{P}$, of components $(\mathrm{d}x_2, \mathrm{d}x_3)$. Let $\boldsymbol{n}$ be the inward normal and v_N be the dissolution rate (i.e. the normal velocity) of the surface element. Examination of Fig. 2 reveals at once that the velocity

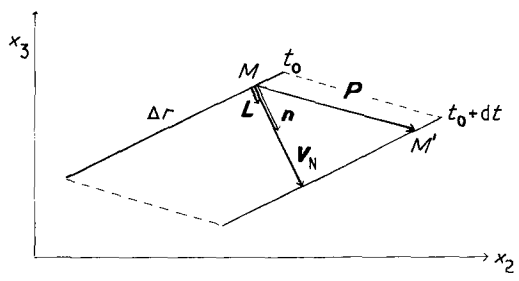

Figure 2 The geometry of the model assuming that $\mathrm{d}t = 1$ sec.

v_3 is not the component along the x_3 axis of a normal velocity vector $\boldsymbol{V}_N$ defined as $\boldsymbol{V}_N = v_N\boldsymbol{n}$.

For this purpose it is pertinent in a second step to introduce a vector associated with a profile element of orientation α and representing a physical quantity we are able to evaluate easily during the dissolution in such a way that the precise knowledge of this vector give us all the information that is needed to determine the propagation vector $\boldsymbol{P}$. An analysis presented in a previous paper [24] demonstrated that the dissolution slowness vector $\boldsymbol{L}$ whose magnitude, L, is the reciprocal of the dissolution rate and whose positive direction coincides with that of the inward normal unit vector $\boldsymbol{n}$ is suitable for both the determination of the propagation vector $\boldsymbol{P}$ and the simulation of the evolution of the dissolution profiles with repeated etchings.

The dissolution slowness vector $\boldsymbol{L}$ with components along the x_2 and x_3 axes respectively given by

$$L_2 = -p/v_3 \tag{5}$$

$$L_3 = 1/v_3 \tag{6}$$

has its extremity which in the (x_2, x_3) plane moves effectively along a polar diagram as the orientation α of the surface element varies. From the definition of the propagation vector $\boldsymbol{P}$ we can demonstrate [24] that the vector $\boldsymbol{T}$ tangent to the polar diagram of $\boldsymbol{L}$ lies perpendicular to the vector $\boldsymbol{P}$. A polar representation of the vector $\boldsymbol{L}$ gives

$$L_2 = f(\beta)\cos\beta \tag{7}$$

$$L_3 = f(\beta)\sin\beta \tag{8}$$

with

$$\boldsymbol{L}\cdot\boldsymbol{L} = (f(\beta))^2 \tag{9}$$

In these equations $\beta = \alpha - (\pi/2)$ is the polar angle of $\boldsymbol{L}$. The relations for $\boldsymbol{P}$ follow from researching the expressions for the components $A(\beta)$ and $B(\beta)$ of the derivative of the rotating vector $\boldsymbol{L}$ with respect to the polar angle β. We finally obtain the following relations [24]

$$\frac{\partial v_3}{\partial p} = \mp\frac{B(\beta)}{(f(\beta))^2} \tag{10}$$

$$\mathrm{d}x_2 = \pm\frac{B(\beta)}{(f(\beta))^2}\,\mathrm{d}t \tag{11}$$

$$\mathrm{d}x_3 = \mp\frac{A(\beta)}{(f(\beta))^2}\,\mathrm{d}t \tag{12}$$

which characterize completely the displacement of a surface profile element within the bulk. The choice between the "+" and the "−" sign is determined by the value of the angle that the vector $\boldsymbol{L}$ makes with its derivative. Thus it is now necessary to know the function $f(\beta)$ which represents the magnitude of the dissolution slowness vector $\boldsymbol{L}$ to track the changes in the shape of the dissolution profile during the dissolution. In the following section we propose a method to express mathematically the magnitude L of the dissolution slowness vector which in three dimensions consists of a tensorial representation of the dissolution slowness.

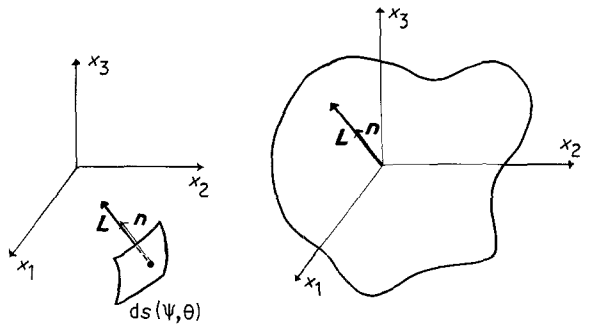

Figure 3 The three-dimensional model. Representation of the dissolution slowness vector, $\boldsymbol{L}$, and of the slowness surface.

2.2. A tensorial representation of the dissolution slowness

We now consider briefly the vectorial analysis in the three-dimensional model. From the preceding section it clearly appears that in three dimensions the dissolution may be described by a dissolution slowness vector $\boldsymbol{L}$ whose magnitude and direction depend on the orientation of a particular surface element, ds, in space (x_1, x_2, x_3). As the orientation of the surface element varies the extremity of the dissolution slowness vector $\boldsymbol{L}$ lies at different points of a representative surface (Fig. 3) denoted for convenience as the slowness surface. The problem is now to find in polar coordinates the equation of the dissolution surface in order to construct the trajectory of a given moving surface element. It must be pointed out that here we adopt the system of notation for designating the orientation of a crystalline surface specified in the IEEE standard on piezoelectricity [25]. In this convention two rotations suffice to define the orientation of the surface element, the first rotation, Ψ, is about the Z axis while the second rotation of θ is about the crystallographic X axis (Fig. 4). The equation representing the slowness surface is therefore a function of the variables Ψ and θ. However examination of Fig. 3 shows that it is also pertinent to choose for alternative variables the three cartesian components, n_i, of the unit inward normal $\boldsymbol{n}$ of the surface element. The orientation of the moving surface element at a given point is effectively known as soon as the three components n_i which depend only on the rotation angles, (Ψ, θ) are determined. Thus an alternative form of the representative equation of the slowness surface is

$$L = F(n_1, n_2, n_3) \tag{13}$$

since a picture of the slowness surface follows the evaluation of the magnitude, L, of the dissolution slowness vector $\boldsymbol{L}$ for all possible values of the components n_1, n_2, n_3 of the inward normal.

At first sight a rigorous mathematical treatment of the three-dimensional dissolution problem seems intractable. However an approximate solution which provides valuable information is obtainable using a polynomial representation of the function F in which three variables n_1, n_2 and n_3 are involved. Thus we can write

$$\begin{aligned} L = {} & D_0 + a_1 n_1 + a_2 n_2 + a_3 n_3 + b_1 n_1^2 \\ & + b_2 n_2^2 + b_3 n_3^2 + b_4 n_2 n_3 + b_5 n_1 n_3 \\ & + b_6 n_1 n_2 + c_1 n_1^3 + \ldots \end{aligned} \tag{14}$$

In fact it is more convenient to rewrite Equation 14 in the more compact form

$$\begin{aligned} L = {} & D_0 + D_i n_i + D_{ij} n_i n_j + D_{ijk} n_i n_j n_k \\ & + D_{ijkl} n_i n_j n_k n_l + \ldots \end{aligned} \tag{15}$$

in which clearly the coefficients D_0, D_i, D_{ij}, D_{ijk}, D_{ijkl}, . . . are components of tensors of rank 0, 1, 2, 3, 4, . . . In a general way these tensors are designated as dissolution tensors.

Since in a N-order polynomial representation one cannot distinguish the product of components $n_i^\alpha n_j^\beta n_k^\gamma$ (with $N = \alpha + \beta + \gamma$) from the product $n_j^\beta n_i^\alpha n_k^\gamma$ it appears that the N subscripts can be interchanged without modifying the values of the tensor coefficient. Moreover the N-subscript dissolution constants refer to the cartesian axes (Fig. 4) and some of them may be zero due to symmetry. Hence the reduction in the number of dissolution constants D_0 up to D_{ijklmn} is performed here by considering the degree of symmetry of quartz crystals. Since a quartz crystal is distinguished by an axis (the crystallographic X axis denoted here as the cartesian x_1 axis) of twofold symmetry and by an axis (the crystallographic Z axis or the cartesian x_3 axis) of threefold symmetry the two following coordinates transformations are to be made.

(1) The transformation concerned with the twofold symmetry in which the component n_i' of the primed inward normal $\boldsymbol{n}'$ in the new rotated system are expressed in terms of the components n_i referred to the x_1, x_2, x_3 axes as

$$n_1' = n_1 \quad n_2' = -n_2 \quad n_3' = -n_3 \tag{16}$$

(2) The threefold symmetry operation in which the orientation of the new axes is specified by the following transformation matrix

$$\begin{array}{c|ccc} & 1 & 2 & 3 \\ 1' & C & S & 0 \\ 2' & -S & C & 0 \\ 3' & 0 & 0 & 1 \end{array} \tag{17}$$

where $C = \cos 120°$ and $S = \sin 120°$.

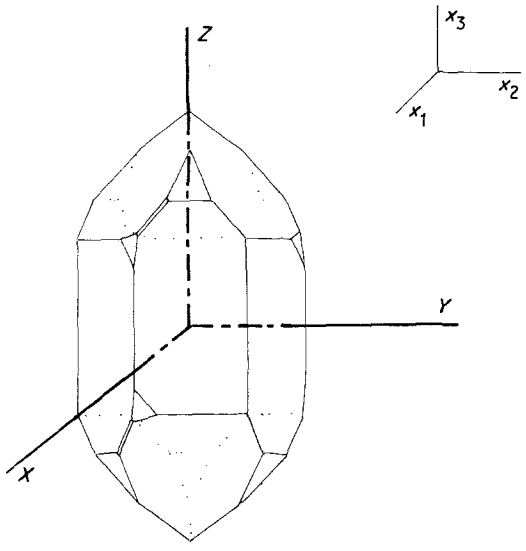

Figure 4 The doubly rotated quartz plates.

TABLE I The independent coefficients of the dissolution tensor of rank N for the trigonal class 32. Except for the tensors of rank 0 and 1, the number of dissolution constants is always greater than the number, v, of independent coefficients

N	v	Identification of the independent coefficients:
0	1	D_0
1	0	
2	2	D_{11}, D_{33}
3	1	D_{111}
4	4	D_{1111}, D_{1123}, D_{1133}, D_{3333}
5	2	D_{11111}, D_{11133}
6	6	D_{111111}, D_{111123}, D_{111133}, D_{112333}, D_{113333}, D_{333333}

The rather cumbersome calculations are performed up to the sixth-order tensor. As an example the calculations necessary to determine the independent coefficients of the dissolution tensor of rank 5 are indicated in Appendix A. The relevant results are displayed in Table I. We observe that in general tensors of odd rank have only a few independent coefficients, for example tensor of rank 5 has only two independent dissolution constants. In contrast the number of independent dissolution constants increases to 6 for the sixth-order tensor.

If the restriction on the dissolution constants is taken into account the general form of Equation 14 reduces to

$$\begin{aligned} L &= D_0 + D_{11}(n_1^2 + n_2^2) + D_{111}n_1(n_1^2 - 3n_2^2) \\ &\quad + D_{1111}(n_1^2 + n_2^2)^2 + D_{3333}n_3^4 \\ &\quad + 6D_{1133}n_3^2(n_1^2 + n_2^2) + 4D_{2223}n_2n_3 \\ &\quad \times (3n_1^2 - n_2^2) + D_{11111}n_1(n_1^2 + n_2^2)(n_1^2 - 3n_2^2) \\ &\quad + 10D_{11133}n_1n_3^2(3n_2^2 - n_1^2) + D_{111111}(n_1^2 + n_2^2)^3 \\ &\quad - 10D_{111123}n_2n_3(n_2^2 + n_1^2)(n_2^2 - 3n_1^2) \\ &\quad + 15n_3^2(n_1^2 + n_2^2)D_{111133} + 20n_2n_3^3 \\ &\quad \times (3n_1^2 - n_2^2)D_{112333} + 15n_3^4(n_1^2 + n_2^2)D_{113333} \\ &\quad + n_3^6D_{333333} \end{aligned} \tag{18}$$

if we limit our investigation to tensor of rank 6.

For a surface obtained by a double rotation of the reference Y-cut plate [25, 26] and specified by the angles of rotation (Ψ, θ) the components of the inward normal to the surface can be expressed as

$$\begin{aligned} n_1 &= \sin \Psi \cos \theta \\ n_2 &= -\cos \Psi \cos \theta \\ n_3 &= -\sin \theta \end{aligned} \tag{19}$$

Substituting into Equation 19 yields the following relation

$$\begin{aligned} L &= L_0 + \sum_j A_j \cos^j\theta + \sum_k B_k \cos^k\theta \sin 3\Psi \\ &\quad + \sum_l C_l \cos^l\theta \sin\theta \cos 3\Psi \end{aligned} \tag{20}$$

where for convenience a shortened notation is used and where the coefficient A_j, B_k and C_l are expressed in terms of the dissolution constants. When we restict our calculations to tensor of rank 6 the subscripts j and l cannot take values which exceed respectively 6 and 5. Moreover for the second term of Equation 20 the subscript will be even while for the other terms the subscript will be odd.

It should be pointed out that from a mathematical point of view the discrepancy between the exact formulation and the approximate Equation 14 may be seriously reduced by extending the tensorial representation to tensors of very high order. Such a consideration justifies the use of the shortened notation of Equation 20; this form becoming very convenient in specific numerical applications.

The above equation involves the coefficients L_0, A_j, B_k and C_l. Evaluation of these coefficient requires a great number of experimental measurements on the dissolution rate of differently oriented quartz plates. In this paper the dissolution slowness, L, is measured for various singly rotated quartz plates. Data on at least 30 differently oriented quartz plates are collected. Hence, in the following section, as an example of the general model the solutions L_0, A_j and C_l of the system of linear equations of the general reduced form

$$L = L_0 + \sum_j A_j \cos^j\theta + \sum_l C_l \sin\theta \cos^l\theta \tag{21}$$

with 16 unknowns are presented. The adequacy of this tensorial representation of the dissolution slowness is then discussed in terms of the shape of the Z' dissolution profiles which are formed on singly rotated surfaces during prolonged etching.

3. Results

3.1. Experimental results

The resonators used were synthetic planoconvex quartz plates. A singly rotated quartz plate with a negative angle θ equal to $-\alpha$ degrees is denoted BT-α. Similarly an AT-β cut corresponds to a positive value of β degrees for the angle of rotation θ. Before etching the various "AT" and "BT" plates were lapped with a 5 μm abrasive. These plates were etched in a concentrated ammonium bifluoride solution (typical concentration 10.5 mol l^{-1}) at a constant temperature in the range 290–360 K for successive periods of time of 30 min. Two procedures were used to characterize after any time of etching the surface texture of etched plates. Firstly surface topography data were determined from profilometry traces given by a microprocessor-based surface profilometer. In particular the traces were made along the rotated Z' direction which lies in the plane surface of singly rotated resonators. Complementary observations on the topography of etched surfaces were obtained by scanning electron microscopy.

3.2. The dissolution rate

For a thin plate (about 1 mm thick for 13.2 mm in diameter) it is reasonable to identify the normal dissolution rate, v_N, with the change in the decrement of thickness, Δd, with the etching time t. Effectively, previous studies [11, 27] have shown that at a given etching temperature T, the changes in the thickness are linear with time t. Hence it is possible to evaluate the dissolution rate, v_N, from frequency measurements. If the resonance frequency, f, of a quartz plate

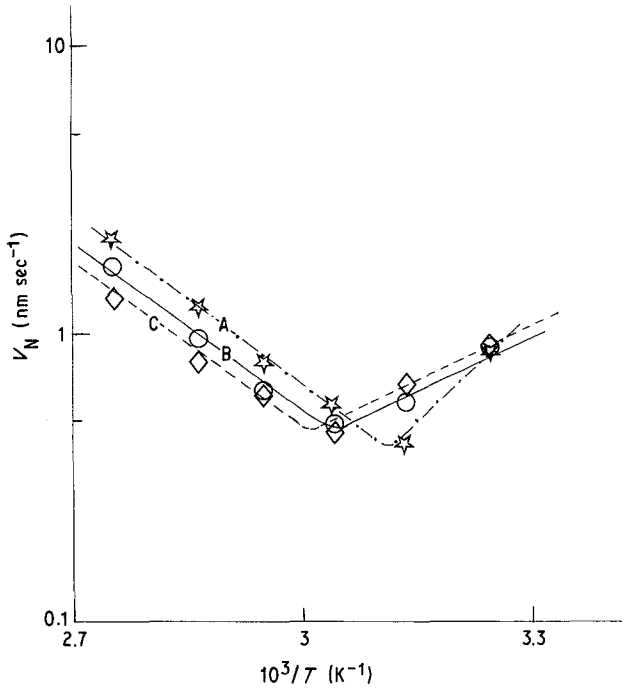

Figure 5 Plot of $\mathrm{Ln}v_N$ against T^{-1} for various singly rotated quartz plates. Curves, A, B, C are respectively for the BT-21, BT-31 and BT-36 plates.

in thickness shear vibration is related to the thickness, d, of the quartz plate by the equation

$$f = Kd^{-1} \tag{22}$$

where K is a constant depending on the cut and on the overtone, it is easy to see that logarithmic differentiation of Equation 21 gives the decrement in thickness as

$$\Delta d = -K\frac{\Delta f}{f_i f_f} \tag{23}$$

where $\Delta f = f_f - f_i$ is the change in frequency owing to the chemical attack.

Following the above procedure the normal dissolution rates were evaluated from the temperature slope of the linear variation of Δd with t in order to plot the data in the form v_N against $1/T$. Data illustrated in Fig. 5 are fitted approximately by a pair of straight lines. The particular behaviour for freshly lapped plates is in general understood [10, 11, 27, 28] in terms of an enhancement of the etch rate for the lower etching temperatures due to a strained surface layer produced by mechanical lapping.

Owing to the influence of the initial surface damage and to avoid some difficulties, the dissolution rate, v_N, was finally measured for the various cuts by extrapolating the Arrhenius plots at a constant reciprocal temperature of $2.7 \times 10^{-3}\ \mathrm{K}^{-1}$. For the orientation θ in the range $-60°$ to $60°$ the normal dissolution rate, v_N, are found to vary by a factor of 7 from one orientation to another. Non-symmetric oscillations in the dissolution rate, v_N, and consequently in the dissolution slowness, L, are observed. Moreover the dissolution slowness reaches the highest value for the Y-cut specimen in agreement with previous experiments [13, 16, 29]. This set of data although not complete allows us to make a tentative attempt to evaluate the constants, L_0, A_j and C_l appearing in the system of Equations 21. At this stage a first representation of the polar diagram of L is possible for angle θ in the range $-60°$ to $60°$. Difficulties might arise when θ approaches a value close to $90°$ or $-90°$. The explanation is probably due to some inaccuracy in the determination of coefficients of high order. Unfortunately the lack of complete experimental data in the ranges $-90° < \theta < -50°$ and $50° < \theta < 90°$ does not help us to give a correct estimate of these high order coefficients.

The rather complicated shape of the experimental polar diagram as derived from Equation 21 using coefficients evaluated up to 16th-order may be seen in Fig. 6a. Some typical values of the angle θ corresponding crudely to a minimum or a maximum of the dissolution slowness, L, are also indicated in this figure. To give a rough experimental verification of the efficiency of the present method experimental values of L are displayed on the polar diagram in Fig. 6b. For θ in the range investigated here the data touch more and less the polar diagram showing that this diagram is crudely comparable with that one can reasonably expect from the data.

3.3. The Z' profilometry traces

A description of the changes in the shape of the Z' profiles produced by dissolution was achieved by profilometry traces made at different etching times. Figs 7 and 8 picture the evolution of the profilometry traces of two different "BT" cuts with the depth,

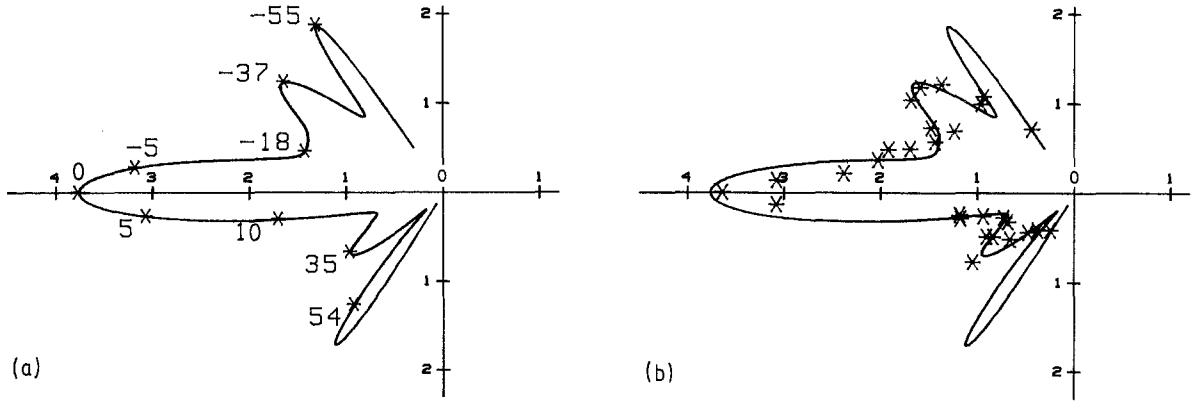

Figure 6 (a) The experimental polar diagram of L in the plane YZ. Some typical values of the angle of rotation θ are indicated in the figure. (b) Experimental fit of the polar diagram; data (*) are essentially collected for θ in the $(-60°, 60°)$ range.

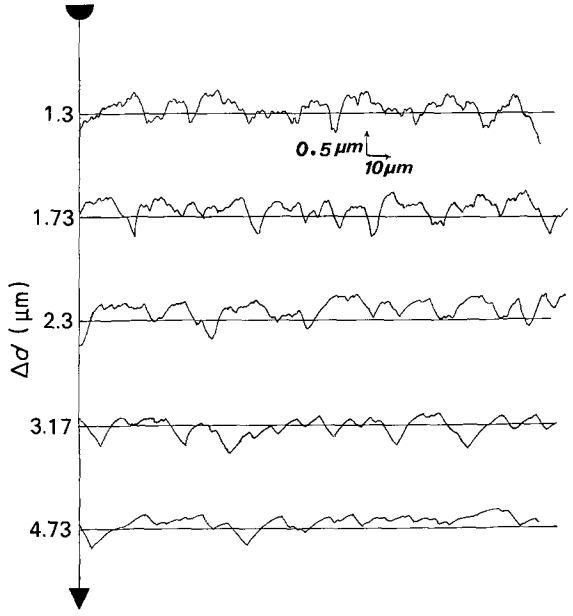

Figure 7 Changes in the surface profilometry traces made along the Z' axis with the depth, Δd_S, of etch of a BT-31 plate.

$\Delta d_S = \Delta d/2$, of etch. From Figs 7 and 8 some essential features are typified.

(1) After a critical depth of etch was reached the Z' dissolution profiles for a given cut remain stable in shape.

(2) The shape of the etch profile is characteristic to the crystal orientation.

(3) For typical orientations repeated etchings result in a more or less pronounced enlargement of the dissolution profiles along the Z' axis.

Hence to establish the consistency of the present model we only need to collect information on the topography of various deeply etched quartz plates which reflect the influence of the orientation on the final shape of the Z' dissolution profiles. This may be seen in Fig. 9 which illustrates some typical results on the Z' profiles of different "BT"-cut plates with θ varying from 0° to −46°. For the $NH_4F \cdot HF$ etchant

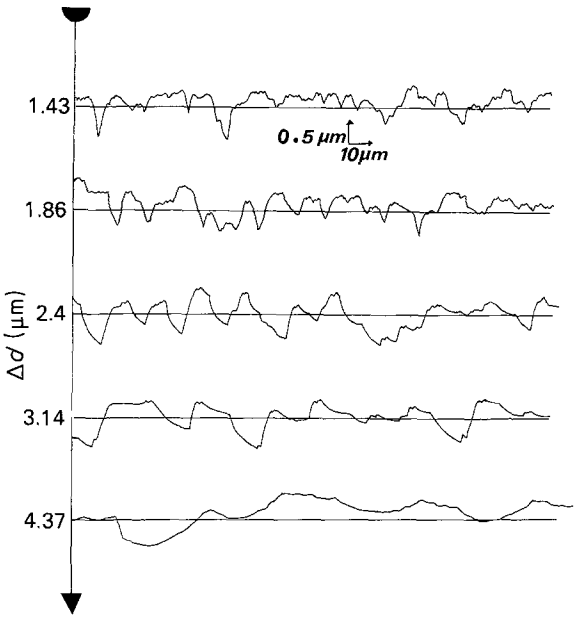

Figure 8 Changes in the surface profilometry traces made along the Z' axis with the depth, Δd_S, of etch of a BT-36 plate.

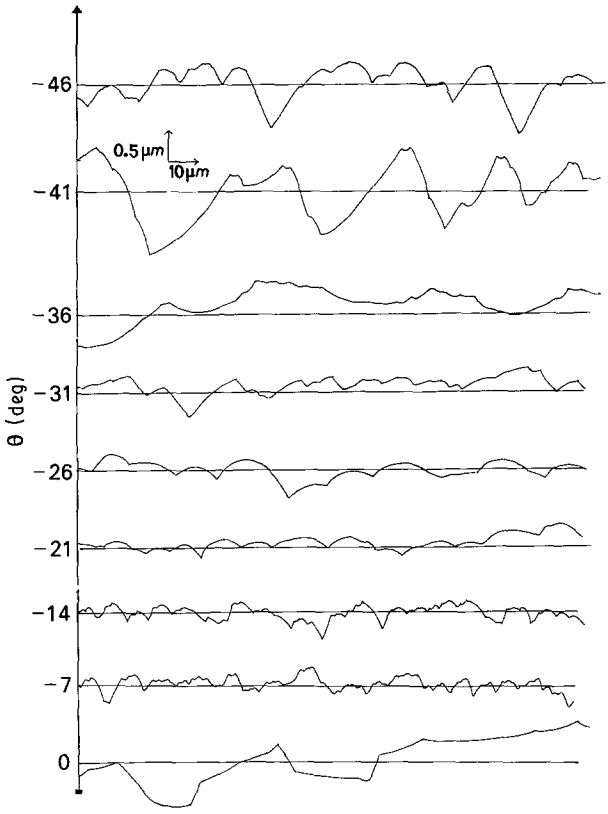

Figure 9 The final Z' traces of differently oriented BT-cut plates.

we observe that a little change of a few degrees in the orientation θ gives rise to a rapid variation in the final shape of Z' profiles. Similar behaviour occurs for the "AT" plates where the angle of cut θ acts as a very sensitive property for the surface texture which develops on deeply etched AT-cut plates [12]. In particular (Fig. 10) the final shape of Z' traces varies continuously from convex to concave and from concave to convex again as the orientation θ of AT-cut plates increased from 29° to 49°.

Since with prolonged etching distinctive etch figures are formed on differently oriented quartz plates, the crystal orientation seems to govern the dissolution process and causes without ambiguity the development of Z' profiles of various shapes. In these

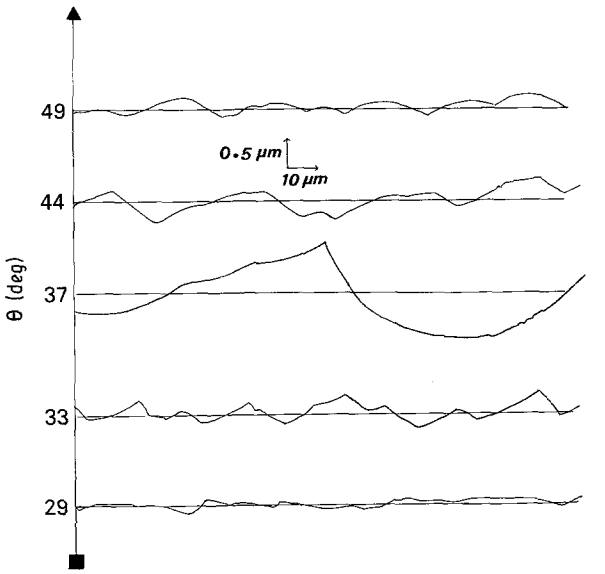

Figure 10 The final Z' traces of differently oriented AT-cut plates.

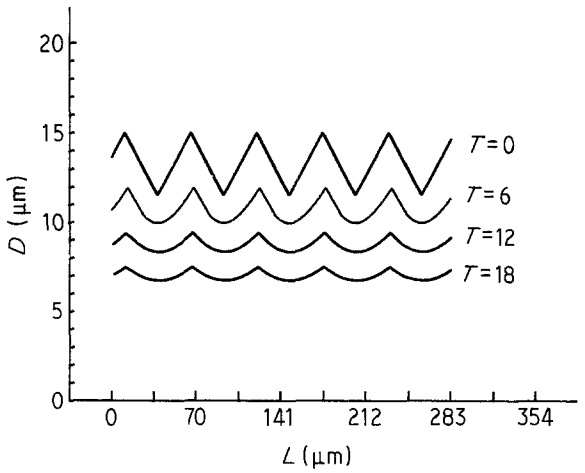

Figure 11 The theoretical changes in the shape of an initial triangular surface profile. The case where $\theta = 0°$.

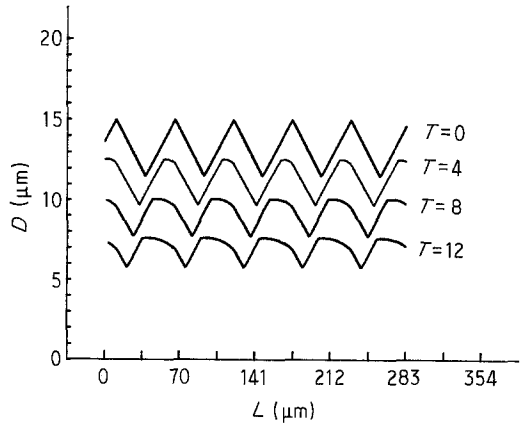

Figure 13 As Fig. 11 for $\theta = -14°$.

conditions the model presented in the above section based on the orientation effect may certainly apply. Thus it is now appropriate to treat the changes in shape of the Z' profile with orientation in terms of this model assuming that the variations of the dissolution slowness with its polar angle is conveniently represented by the polar diagram in Fig. 6a.

3.4. The numerical simulation

In view of the experimental results pictured in Figs 9 and 10 interest in a graphical approach of the etching problem is revived. For this purpose we have developed a numerical simulation [24] which allows us to follow graphically the evolution with a prolonged etching of either an initial triangular profile or a surface profile with an initial randomized shape. The program which evaluates the cartesian components of the propagation vector, $\boldsymbol{P}$, starting from the polar diagram of $\boldsymbol{L}$ has been described elsewhere [24]. Here it is sufficient to note that the Z' profiles of differently oriented quartz plates which all lies in the x_3x_2 plane are associated with a dissolution slowness vector $\boldsymbol{L}$ whose polar diagram may be represented by Equation 21.

To compare the predictions of the present model with the experimental results and especially to verify the interest in the tensorial method as a mathematical procedure to determine experimentally the polar diagram of $\boldsymbol{L}$ we have chosen here, for the sake of simplicity, to deal essentially with an initial triangular profile.

Theoretical results for the BT-cut plate with angle θ ranging from 0° to −46° are displayed in Figs 11 to 19. In the past Irving [30] noticed that certain etch rate–orientation relationships give rise to typical surface textures. In particular when the reference surface corresponds to a maximum of the etch rate, i.e. to a minimum of the dissolution slowness, a convex background is formed. Conversely a maximum of the dissolution slowness, L, results in the development of a concave background structure. Examination of Figs 14 and 17 shows that these predictions are verified for BT-cuts with an angle θ respectively close from −20° and −36°. We also observe that if the reference orientation is situated midway between the reference orientation θ_1 and θ_2 corresponding successively to a minimum and to a maximum of L the section of the resultant etched surface are found to exhibit a shape alternately convex and concave as evidenced for example by Fig. 16.

Simulation of the etching of AT-cut plates leads (Figs 20 to 23) to the formation of Z' dissolution profiles whose configuration is also indicative of the positions of the maximum or/and of the minimum of the dissolution slowness with respect to the crystal surface.

4. Discussion and conclusion

Comparison of the final profilometry Z' traces of differently oriented BT-cut plates (Figs 7 to 9) with the

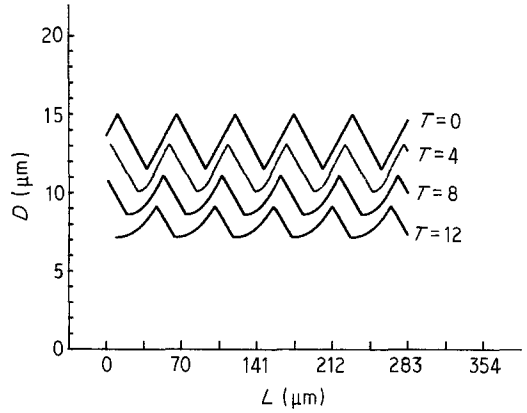

Figure 12 As Fig. 11 for $\theta = -7°$.

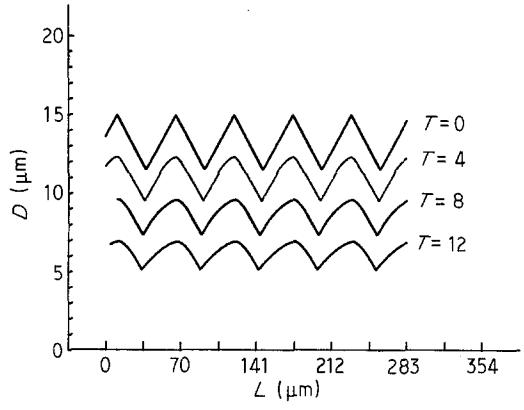

Figure 14 As Fig. 11 for $\theta = -20°$.

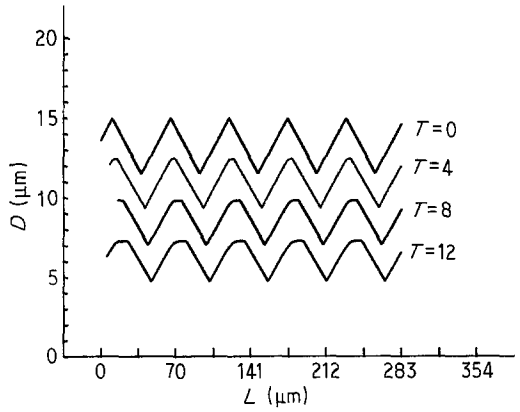

Figure 15 As Fig. 11 for $\theta = -26°$.

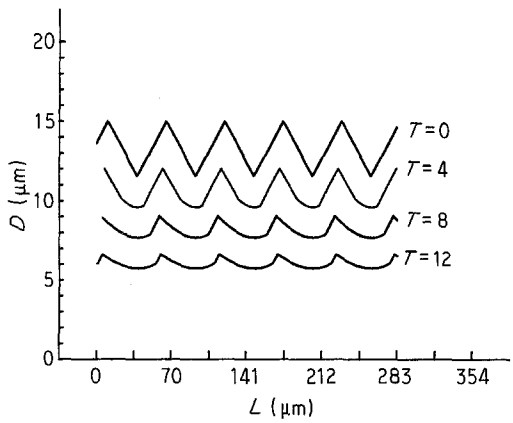

Figure 17 As Fig. 11 for $\theta = -36°$.

final dissolution profiles (Figs 11 to 19) derived from the numerical simulation shows a very satisfactory agreement. This agreement could be exploited to obtain some interesting information. For example, the clear correspondence which exists between the quasi-rounded shape of the dissolution profiles depicted respectively in Figs 14 and 15 and the experimental profiles of Fig. 9 indicates that a relatively flat minimum of the dissolution slowness will certainly occur for θ around $-24°$. Moreover study of Z' profilometry traces of deeply etched BT-31 and BT-41 plates and comparison with the results of the numerical simulation displayed in Figs 16 and 18 respectively also yield reliable results; similar alternate shapes are effectively observed for the quartz surfaces and for the triangular-like surface etched down to 5–6 μm. In particular we believe that the dissolution slowness increases to a maximum for θ around 37° and falls to a minimum for $\theta = 49°$ in relative agreement with the experimental polar diagram. This one-to-one correspondence significantly contributes to the determination of the positions of minima and maxima of the dissolution slowness [24]. The most useful information compiled from the systematic comparison of the theoretical results with the true final Z' traces of BT-cut plates are listed in Table II.

It is also of interest to discuss briefly some results on the AT-cut plates. Other examples of a successful approach in the prediction of the shape of the dissolution profiles can be considered first. The theoretical final profiles depicted in Figs 21, 22 and 23 look roughly identical to the experimental ones (Fig. 10).

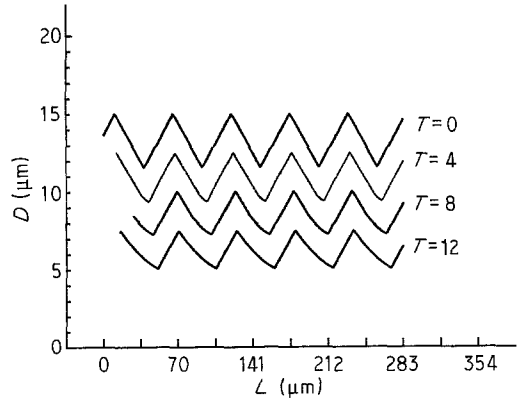

Figure 16 As Fig. 11 for $\theta = -31°$.

This provides a rapid identification of the positions of some minima and maxima of L (Table II). However, the theoretical results for the AT-cut plates with angle $18° \leqslant \theta < 31°$ have been found to be generally not as good as the results for BT-cut plates (see for example Fig 20). We have previously established [24] that the shape of the etched profile is essentially determined by the "distance" in degrees of the reference surface from a minimum or a maximum etch rate plane. Hence, the observed deviations may be attributed to a false positioning (about 9°) of a minimum of the dissolution slowness which in reality lies within the range $24° < \theta < 28°$ rather than in the vicinity of 18° as evidenced by Fig. 6a. This erroneous displacement of at least 6° will certainly alter the shape of the theoretical etched profiles. However, translating this minimum of the dissolution from about 18° to about 26° may certainly improve the predictions of the numerical simulation. At this point it should be noticed that in the present work we investigated the chemical etching at AT plates cut in various quartz bars either synthetic or natural. Only data on BT plates are collected from plates cut in the same synthetic quartz crystal.

Since various quartz crystals certainly have different bulk properties affecting to some degree the rate of the chemical attack [30, 31], it is possible for a same angle, θ, of rotation but for plates made from various crystals to observe differences in the measured etch rates. Specific deviations of about 20% have been effectively obtained for standard AT-cut plates ($\theta = 35°30'$) using synthetic and natural quartz crystals [10]. These deviations are sufficient to limit

TABLE II Theoretical and experimental values of the minima and the maxima in the dissolution slowness as derived respectively from the polar diagram (Fig. 6a) and from the experimental changes in the shape of the final Z' trace with orientation

	BT-cut plates, angle θ in degrees	AT-cut plates, angle θ in degrees
Theoretical minima	Flat minimum from $-20°$ to $-25°$; $-45°$	18°; 48°
Theoretical maxima	0°, $-36°$, $-57°$	37°; 59°
Experimental minima	Flat minimum from $-21°$ to $-26°$, $-46°$	25°; 49°
Experimental maxima	0°, $-36°$	38°

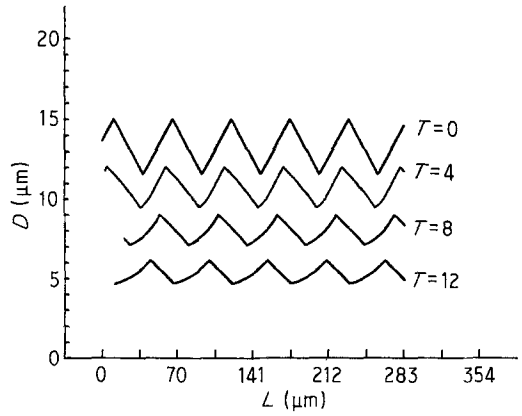

Figure 18 As Fig. 11 for $\theta = -41°$.

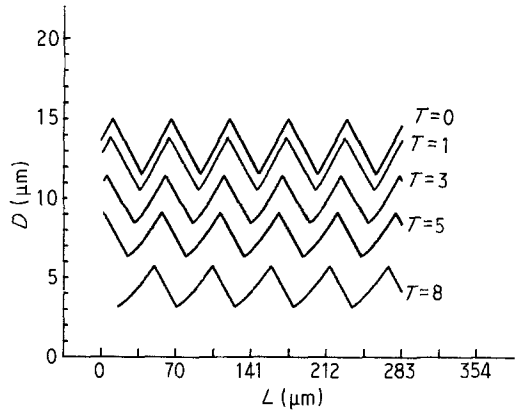

Figure 20 As Fig. 11 for $\theta = 29°$.

considerably the accuracy of the tensorial method. However it might be of interest to note that successive tentative attempts to fit more accurately the polar diagram of L for positive values of the rotation angle using the experimental data does not cause a marked displacement of the positions of "extrema" of L related to BT-cut plates. Only the amplitude of the extrema is altered. Thus to minimize error in the experimental drawing of the polar diagram of L it seems necessary to perform measurements on plates cut in the same synthetic quartz bar. However, selecting and designing at least 50 resonators with orientation θ varying slowly from $-70°$ to $70°$ remain a considerable task and require a crystal of relatively large dimensions. This explains why in practice the data are partly obtained with different specimens.

Moreover if we regard the case where we substitute an initial randomized surface profile to the triangular profile (Figs 24 and 25) it appears as expected that the final shape of the dissolution profiles is not affected by the nature of the initial profile. A final quasi-concave background structure develops on the BT-36 plate while a final Z' profile of alternative shape is formed on the BT-31 surface in close agreement with the shapes of profiles depicted in respective Figs 16 and 17.

It is also of interest to discuss briefly some results on the variation of the dissolution rate with the angle θ of rotation. Effectively it is possible to evaluate the dissolution rate from the theoretical dissolution profiles. For this, since the length and the position of successive profile elements vary continuously during the etching, we have chose to compute a centre line for any dissolution profile by a sampling method [32]. For this, we define a very short sampling length and the profile is split into a number of sampling lengths, l_S, for each of which, firstly new coordinates (x_2, x_3) of a profile element are calculated and secondly, a separate mean line is computed. Note that for a typical sampling length of $0.2\,\mu m$ the effective dissolution profile remains graphically unchanged to the human eye by the sampling. The consecutive depths of etch, Δd_L, are then taken as the distances, at given abscissae, between the mean lines related respectively to the initial profile and to the etched profile. The average depth of etch, Δd_S, corresponds to the mean of Δd_L of all consecutive sampling lengths. We can then easily evaluate the "theoretical" dissolution rate which is defined as the ratio of the average depth of etch to the etching time. Moreover for these calculations we have preferred to start from a profile of initial randomized shape we expect to represent more accurately a lapped surface (see, for example, Figs 20 and 21). From values related to BT plates, Table III has been constructed for a rapid comparison. The agreement with experiments is rather good except for the apparently anomalous behaviour of the BT-7 plate which requires confirmation by additional experimental measurements. In general where there are deviations they do not exceed 10%. Moreover the fact that a large deviation occurs at $\theta = -7°$ is not really surprising. The correlation between the final Z' trace of the BT-7 plate (Fig. 9) and the theoretical dissolution profile (Fig. 12) seems not so clear as for other BT-cut plates. Hence it is not easy to be sure that the anomaly is caused solely by inaccuracies in the measurements of the dissolution rate. Perhaps, we need to take the polynomial regression to higher orders still; but as

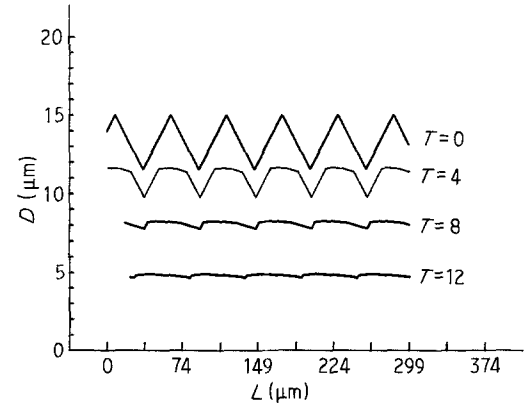

Figure 19 As Fig. 11 for $\theta = -46°$.

TABLE III Values of the ratio, v_{Nexp}/v_{Nth}, for differently oriented BT plates. v_{Nexp} and v_{Nth} refer respectively to experimental values and theoretical values of the dissolution rate

θ (deg)	v_{Nexp}/v_{Nth}
0	0.9
−7	1.75
−14	0.92
−21	0.98
−26	1.11
−31	0.98
−36	0.93
−41	0.94
−46	1.08

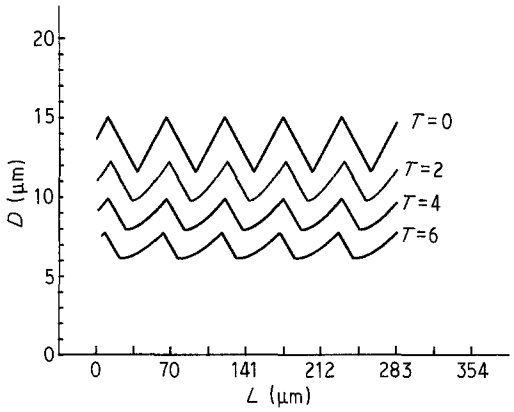

Figure 21 As Fig. 11 for $\theta = 33°$.

noticed in this case difficulties in the experimental work can restrict the supply of complementary reliable data. However, one can consider this deviation accidental since for BT-cut plates this model leads to properties (changes in etch rate with orientation, surface features) quite similar, qualitatively and quantitatively, to those observed experimentally.

In view of this excellent correlation we can conclude that, in combination with a vectorial analysis of the dissolution problem, a tensorial representation of the dissolution slowness appears as a recommendable method for quantitative work in study of etched quartz surfaces. Moreover, it should be emphasized that this method becomes particularly valuable when practically qualitative informations on the shape of etched sections of quartz crystals undergoing photolithography and anisotropic etching [32–34] are needed.

For doubly rotated quartz plates the dissolution slowness could vary in a complicated way with the angles of cut. Hence the investigation has not yet been made systematically. However, the results collected here seem sufficient to conclude that this model should provide valuable information about the shape of the dissolution profiles in any direction of any given cut. For this purpose it becomes necessary to perform a great lot of experiments on quartz plates obtained firstly, by rotation of various amounts Ψ about the Z axis and secondly, by rotation of various amounts θ about the Y axis. These experiments are rather fastidious, but the information one obtains is essential and ensures some progress toward the exact geometrical representation of the slowness surface. It is effectively imperative to find the formulation of Equation 20 if we wish to be able to detect theoretically the surface texture of the shape of etched sections of doubly rotated quartz plates. These long investigations will be reported in future papers.

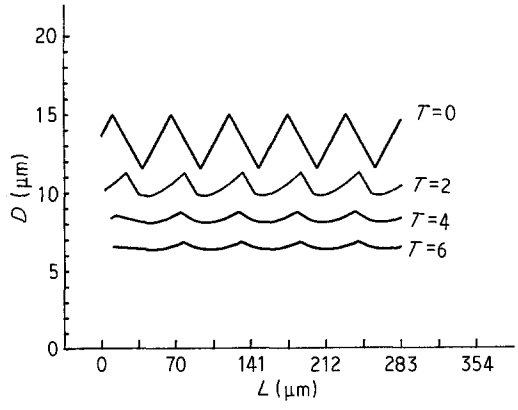

Figure 22 As Fig. 11 for $\theta = 37°$.

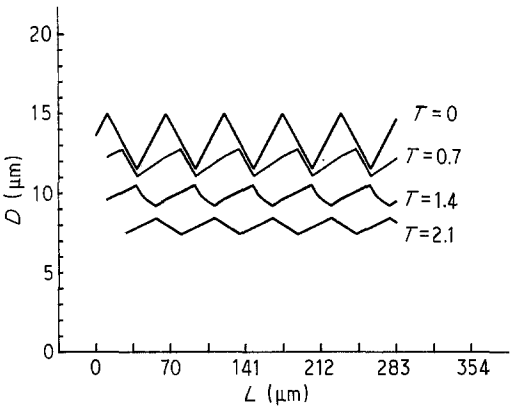

Figure 23 As Fig. 11 for $\theta = 44°$.

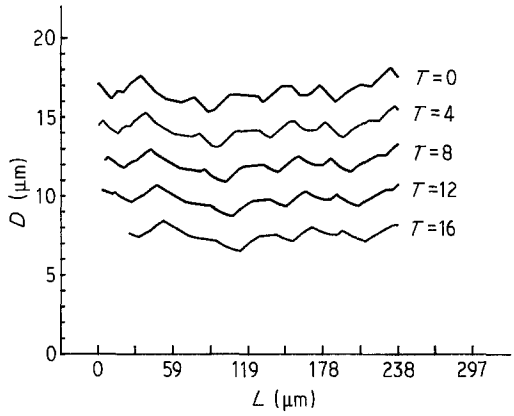

Figure 24 The theoretical changes in the shape of an initial random surface profile. The case where $\theta = -31°$.

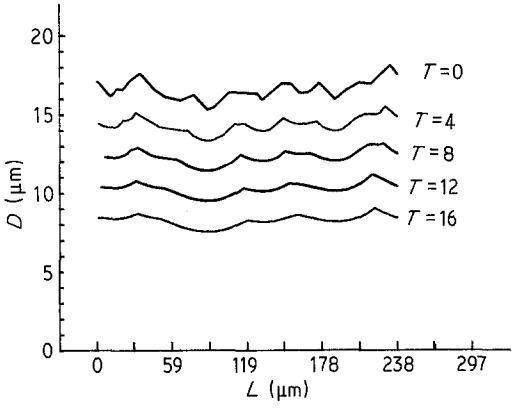

Figure 25 As Fig. 24 for $\theta = 36°$.

Acknowledgements

The authors gratefully acknowledge financial support from the Direction des Recherches Etudes et Techniques which depends on the French Department of Defense.

Appendix: Determination of the independent dissolution constants of the tensor of rank 5

In a transformation from axes (x_1, x_2, x_3) to axes (x'_1, x'_2, x'_3) let the dissolution constants D'_i, D'_{ij}, D'_{ijk} and so on be referred to the primed system of arbitrary orientation.

A1. Reductions due to the twofold axis

We start with the axes x'_1, x'_2, x'_3, coinciding with the reference axes and consider a transformation defined by a rotation of the primed axes through an angle of 180° about the x_1 axis. This determines a transformation which in accord with the two-fold symmetry brings the crystal into an equivalent position with regard to its structural position. Hence here the dissolution constants are in no way affected thereby. Thus with respect to this specific transformation the dissolution constants which do not vanish are the following

$$D_{11111}, D_{11122}, D_{11123}, D_{11133}$$

$$D_{12222}, D_{12223}, D_{12233}, D_{12333}, D_{13333}$$

They evidently involve an even number of subscript 2 or/and 3.

A2. Reductions due to the threefold axis

Now we consider the transformation where the direction cosines, a_{ij}, for this transformation are

$$\begin{matrix} C & S & 0 \\ -S & C & 0 \\ 0 & 0 & 1 \end{matrix}$$

where $C = \cos(120°)$ and $S = \sin(120°)$.

The primed dissolution coefficients D'_{ijklm} referred to this particular transformation are readily identified as equivalent to the dissolution constant D_{ijklm} referred to the reference axes x_1, x_2, x_3.

One can now convert the five-subscript coefficient by applying the usual transformation rule for fifth-order tensor

$$D'_{ijklm} = a_{in}a_{jo}a_{kp}a_{lq}a_{mr}D_{nopqr}$$

For dissolution constants involving subscripts equal to 1 and/or 2 we obtain equations of the form

$$\begin{aligned} (C^5 - 6C^3S^2 + 3CS^4 - 1)D_{11122} \\ + (3C^3S^2 - 2CS^4)D_{12222} + C^3S^2D_{11111} &= 0 \\ (6C^2S^3 - 3C^4S - S^5)D_{11122} \\ + (2C^4S - 3C^2S^3)D_{12222} - C^2S^3D_{11111} &= 0 \\ 10C^2S^3D_{11122} + 5C^4SD_{12222} + S^5D_{11111} &= 0 \end{aligned}$$

This system of three equations yields the following relations between the coefficients D_{11111}, D_{11122} and D_{12222}

$$\begin{aligned} 3D_{11111} &= -5D_{12222} \\ D_{11111} &= -5D_{11122} \end{aligned}$$

Turning to the dissolution constants D_{11133} annd D_{12233} the transformation rule provides the two equations

$$\begin{aligned} (C^3 - 1)D_{11133} + 3CS^2D_{12233} &= 0 \\ CS^2D_{11133} + (C^3 - 1 - 2CS^2)D_{12233} &= 0 \end{aligned}$$

for the two unknowns. We readily find the relation

$$D_{11133} = -D_{12233}$$

It is left as an exercise for the reader to show that the dissolution constants D_{11123}, D_{12223}, D_{12333} and D_{13333} must be zero.

References

1. J. VIG, H. WASSHAUSEN, C. COOK, M. KATZ and E. HAFNER, Proceedings 27th Annual Symposium on Frequency Control, Fort Monmouth, N.J, 1973 (Electronic Industries Association, Washington, DC, 1973) p. 98.
2. J. R. VIG, J. W. LEBUS and R. FILLER, Report ECOM-4548, 1977 (US Army Electronics Command, Fort Monmouth, NJ).
3. J. R. VIG, C. F. COOK, K. SCHWIDTAL, J. W. LEBUS and E. HAFNER, Proceedings 28th Annual Symposium on Frequency Control, Fort Monmouth, NJ, 1974 (Electronic Industries Association, Washington, DC, 1974) p. 96.
4. J. R. VIG, R. J. BRANDMAYR and R. L. FILLER, Proceedings 33rd Annual Symposium on Frequency Control, Fort Monmouth, NJ, 1979 (Electronic Industries Association, Washington, DC, 1979) p. 351.
5. R. J. BRANDMAYR and J. R. VIG, Proceedings 39th Annual Symposium on Frequency Control, Philadelphia, Pa, 1985 (IEEE, New York, 1985) p. 276.
6. D. ANG, Proceedings 32nd Annual Symposium on Frequency Control, Fort Monmouth, NJ, 1978 (Electronic Industries Association, Washington, DC, 1978) p. 282.
7. A. J. BERNOT, Proceedings 38th Annual Symposium on Frequency Control, Philadelphia, Pa, 1985 (IEEE, New York, 1985) p. 271.
8. Y. SEKIGUCHI and H. FUNAKUBO, *J. Mater. Sci.* **15** (1980) 3066.
9. H. FUKUYO and N. OURA, Proceedings 30th Annual Symposium on Frequency Control, Fort Monmouth, NJ, 1976 (Electronic Industries Association, Washington, DC, 1976) p. 254.
10. C. R. TELLIER, *Surf. Technol.* **21** (1984) 83.
11. C. R. TELLIER and C. BURON, *ibid.* **22** (1984) 287.
12. C. R. TELLIER, Proceedings 38th Annual Symposium on Frequency Control, Philadelphia, Pa, 1984 (IEEE, New York, 1984) p. 105.
13. *Idem.*, Proceedings XIth International Congress of Chronometry Besançon, France, 1984 (Société Française des Microtechniques et de Chronométrie, Besançon, 1984) p. 115.
14. *Idem.*, Proceedings 39th Annual Symposium on Frequency Control, Philadelphia, Pa, 1985 (IEEE, New York, 1985) p. 276.
15. C. R. TELLIER and F. JOUFFROY, *J. Mater. Sci.* **18** (1983) 3621.
16. M. CASTAGLIOLA, C. R. TELLIER and J. L. VATERKOWSKI, *ibid.* **21** (1986) 3551.
17. C. R. TELLIER, F. JOUFFROY and C. BURON, *Mater. Chem. Phys.* **14** (1986) 25.
18. C. R. TELLIER and J. L. VATERKOWSKI, *Surf. Technol.* **26** (1985) 275.
19. C. R. TELLIER, N. VIALLE and J. L. VATERKOWSKI, Proceedings 40th Annual Symposium on Frequency Control, Philadelphia, Pa, 1986 (IEEE, New York, 1986) p. 76.
20. C. R. TELLIER, N. VIALLE and J. L. VATERKOWSKI, First European Time and Frequency Forum, Besançon, France, 1987 (Imprimerie du Conseil Général du Doubs, Besançon, 1987) p. 159.
21. R. B. HEIMANN, in "Silicon Chemical Etching", edited by J. Gramaier, (Springer, Berlin, 1982) pp. 197–224.

22. M. J. LIGHTHILL and G. B. WITHAM, *Proc. R. Soc.* **A229** (1955) 281.
23. F. C. FRANK, in "Growth and Perfection of Crystals", edited by R. H. Doremus, B. W. Roberts and D. Turnbull (John Wiley, New York, 1958) pp. 411–419.
24. C. R. TELLIER, N. VIALLE and J. L. VATERKOWSKI, *Surf. Coatings Technol.* **34** (1988) 417.
25. "Standard on Piezoelectricity" (IEEE, New York, 1978) pp. 15–27.
26. P. VIGOUREUX and C. F. BOOTH, "Quartz Vibrators and their Applications" (HMSO, London, 1950) Chap. 7.
27. C. R. TELLIER, *J. Mater. Sci.* **17** (1982) 1348.
28. B. SCHWARTZ and H. ROBBINS, *J. Electrochem. Soc.* **123** (1976) 1903.
29. F. M. ERNSBERGER, *J. Phys. Chem. Solids* **113** (1960) 347.
30. B. A. IRVING, in "The Electrochemistry of Semiconductors", edited by P. J. Holmes (Academic Press, London, 1962) pp. 256–289.
31. K. H. YANG, *J. Electochem. Soc.*, **131** (1984) 1140.
32. T. R. THOMAS, "Rough Surfaces", (Longman, London, 1981) Chap. 4.
33. H. CHOFFAT, 58ème Congrès de la Société Suisse de Chronométrie, Bienne, Switzerland, 1983, Paper No. 8.
34. T. UEDA, F. KOHSAKA and E. OGITA, Proceedings 10th Conference IMEKO an Measurement of Force and Mass, Kobe, Japan, September 1981, pp. 17–22.
35. W. ZINGG, C.N.R.S. Seminar on Frequency Standards, Besançon, 6–7 mars 1985 (Editions due CNRS, Paris, 1985) pp. N-1–15.

Received 14 January
and accepted 1 June 1988